

Assessing the potential of using high spatial resolution daily NDVI-time-series from planet CubeSat images for crop monitoring

Luís Guilherme Teixeira Crusiol, Liang Sun, Ruiqing Chen, Zheng Sun, Dejun Zhang, Zhongxin Chen, Deji Wuyun, Marcos Rafael Nanni, Alexandre Lima Nepomuceno & José Renato Bouças Farias

To cite this article: Luís Guilherme Teixeira Crusiol, Liang Sun, Ruiqing Chen, Zheng Sun, Dejun Zhang, Zhongxin Chen, Deji Wuyun, Marcos Rafael Nanni, Alexandre Lima Nepomuceno & José Renato Bouças Farias (2021) Assessing the potential of using high spatial resolution daily NDVI-time-series from planet CubeSat images for crop monitoring, International Journal of Remote Sensing, 42:18, 7114-7142, DOI: [10.1080/01431161.2021.1939908](https://doi.org/10.1080/01431161.2021.1939908)

To link to this article: <https://doi.org/10.1080/01431161.2021.1939908>



Published online: 09 Aug 2021.



Submit your article to this journal [↗](#)





View related articles [↗](#)



View Crossmark data [↗](#)



Assessing the potential of using high spatial resolution daily NDVI-time-series from planet CubeSat images for crop monitoring

Luís Guilherme Teixeira Crusiol ^{a,b}, Liang Sun^a, Ruiqing Chen^a, Zheng Sun^a, Dejun Zhang^c, Zhongxin Chen^a, Deji Wuyun^a, Marcos Rafael Nanni ^b, Alexandre Lima Nepomuceno^d and José Renato Bouças Farias^d



^aKey Laboratory of Agricultural Remote Sensing, Ministry of Agriculture/CAAS-CIAT Joint Laboratory in Advanced Technologies for Sustainable Agriculture – Institute of Agricultural Resources and Regional Planning, Chinese Academy of Agricultural Sciences, Beijing, China; ^bDepartment of Agronomy, State University of Maringá, Maringá, Brazil; ^cChongqing Institute of Meteorological Sciences, Chongqing, China; ^dEmbrapa Soja (National Soybean Research Centre – Brazilian Agricultural Research Corporation), Londrina, Brazil

ABSTRACT

The agricultural land use combined with agronomic management practices shall be structured on sustainable practices, guaranteeing both the maximization of productivity and environment preservation. NDVI (Normalized Difference Vegetation Index) time-series has been recognized as a useful methodology to monitor crop development and its spatial distribution. However, there is always a trade-off between spatial and temporal resolutions in satellite data. Hence, high spatial and temporal resolutions from Planet CubeSat represent a possibility to overcome this trade-off. This paper investigated the potential of using high spatial resolution daily NDVI-time-series from Planet CubeSat images for crop monitoring. One hundred nineteen images from 2017, at 3 m ground sampling distance, over cotton, spring corn and winter wheat fields, were acquired and converted into NDVI. The harmonic analysis of time series (HANTS) algorithm was applied to obtain a smoothed cloud and gap-free daily time-series. The 3 m daily time-series were resized to daily 9 and 30 m resolution; and resampled to temporal resolutions at 4, 8 and 16 days intervals to assess the impact of spatial and temporal resolution on NDVI time-series. NDVI time-series were evaluated by their minimum, maximum, average and coefficient of variation across the year. Principal component analysis (PCA) and the stepwise procedure were applied to assess optimum features (days across the year) to assist the NDVI-time-series interpretation. PCA and stepwise highlighted the best time across the year for NDVI-time-series interpretation. As the spatial resolution decreases, the range of NDVI and its standard deviation within field also decreases, leading to loss of within field spectral variability. At daily temporal resolution, slight differences in crop development can be detected in a very short time interval, but as the

ARTICLE HISTORY

Received 26 November 2020
Accepted 22 April 2021

CONTACT Liang Sun  sunliang@caas.cn  Key Laboratory of Agricultural Remote Sensing, Ministry of Agriculture/CAAS-CIAT Joint Laboratory in Advanced Technologies for Sustainable Agriculture – Institute of Agricultural Resources and Regional Planning, Chinese Academy of Agricultural Sciences, Beijing 100081, China

temporal resolution decreases the changes in crop development are detected at larger rates. The high temporal and spatial resolutions from Planet CubeSat images demonstrated great potential to monitor agricultural systems and can subsidize, on forthcoming research, the local and regional monitoring of agricultural areas and contribute to better management regarding strategic planning of governmental and corporate decision making over technical issues.

1. Introduction

China is one of the world's largest crop producers and is responsible for 17%, 22% and 23% of world's wheat, corn and cotton production, respectively (USDA 2020). Agricultural farmlands in China are characterized by small-scale individual-owned farmland, usually smaller than 1 ha and highly fragmented in narrow stripes of crop rows (parcels) (Pan et al. 2015; Wu et al. 2018; Hu et al. 2019), which requires fine spatial and temporal resolutions to characterize the land use and its changes through time. In this context, a time-efficient monitoring of crops and their spatial distribution is important for better management of supply regulation, food security, financial market and strategical planning of governmental and corporative decision making over technical issues (de Souza et al. 2015; Song et al. 2017; da Silva Junior et al. 2017; Padhee and Dutta 2019).

One of the most recognized methodologies to attend the efficient crop monitoring and its spatial distribution is the use of satellite-based NDVI time-series (Masialeli, Egbert, and Wardlow 2010; Tsalyuk, Kelly, and Getz 2017; Werner, Oliveira, and Esquerdo 2020). According to Sakamoto (2020), vegetation indices (e.g. NDVI) are used under the assumption of their direct relationship with canopy biomass, which is a response to biotic and abiotic factors, such as weather, nutrient supply, soil water status, diseases and insects over the past days. However, the information capable of being extracted from NDVI-time-series deeply depends on its spatial resolution and revisiting time of the sensor (Liu et al. 2019; Zhang et al. 2020) and also on the analysed cropping system.

When using satellite data to assess crop growing patterns, there is always a trade-off between spatial and temporal resolutions (Sun et al. 2017). Furthermore, the cloud cover on satellite images is a key factor that affects frequency of cloud-free images obtainment. While the spatial resolution plays a role in the identification of more detailed canopy spectral variability, allowing the evaluation of complex landscapes and within field variability, the temporal resolution (with cloud-free images) is important to detect changes through time at the same field, contributing for the understanding of crop phenology and development, making able a time-efficient decision making over crop management. However, sensors with high revisiting frequency, providing daily images on the same field, usually present coarse spatial resolution and, on the other hand, high spatial resolution sensors usually present low revisiting frequency (Sun et al. 2017).

One possibility to overcome the trade-off between spatial and temporal resolution on satellite-based images is the use of multi-satellite data fusion algorithms. Several algorithms have been developed aiming at promoting the fusion of coarse spatial resolution and high revisiting frequency satellites (e.g. MODIS – MODerate resolution Imaging

Spectroradiometer) with fine spatial resolution and low revisiting frequency satellites (e.g. Landsat) (Gao et al. 2006; Zhu et al. 2010, 2016; Li et al. 2017; Liu et al. 2018; Sun et al. 2021). Although data fusion methods represent a way to overcome the trade-off between pixel size and frequency of image, the lack of observation at very high spatial resolution (<5 m) still poses limitations to the obtainment of high-resolution daily time-series (Houborg and McCabe 2016).

By this reason, another possibility is the use of the PlanetScope (PS) Constellation, delivering high spatial resolution images at high revisiting frequency. Planet © (www.planet.com) has launched hundreds of nano-satellites, so-called as CubeSat 3 U, with small size (10 × 10 × 30 cm) and low weight (<4 kg), providing, by its sun-synchronous orbit, daily global nadir-pointing land surface imaging on four spectral bands (red, green, blue and near-infrared) with a 3–4 m nadir ground sampling distance (GSD) (Houborg and McCabe 2018). Since then, the acquisition of an unprecedented dense time-series at a high spatial resolution is contributing for urban, environmental and agricultural monitoring worldwide.

The recently advances in the obtainment of daily high spatial resolution satellite-based images has led to an increasing number of research works addressing the use of Planet CubeSat images for agricultural monitoring (Houborg and McCabe 2016, 2018; Aragon et al. 2018; Poursanidis et al. 2019; Kimm et al. 2020), landscape studies (Huang et al. 2020), water investigations (Cooley et al. 2017; Wicaksono and Lazuardi 2018; Maciel et al. 2020; Li et al. 2019) and natural inventories (Kääb, Altena, and Mascaro 2017; Shao et al. 2019; Aldeghi et al. 2019; Mazzanti, Caporossi, and Muzi 2020), demonstrating the relevance of this product for better understanding land surface process, especially in complex landscapes, where both temporal and spatial resolutions are important.

Based on the current progress, this paper aims at investigating the potential of using high spatial resolution daily NDVI-time-series from Planet CubeSat images for crop monitoring. The specific goals of this paper are: (1) to evaluate crop development through 3 m daily NDVI-time-series; (2) to assess optimum features (days across the year) for NDVI-time-series interpretation; (3) to assess the spatial resolution effect on within field NDVI monitoring; and (4) to evaluate the effect of temporal resolution on data dimensionality and crop development monitoring.

2. Materials and methods

2.1. Study area

The study area comprises the Hengshui City, Hebei Province, China. Three fields, defined in this paper as a portion of land with the same crop type (Figure 1), with area between 9 and 14 ha, containing cotton, spring corn and winter wheat crops with different number of seasons across the year (single and double-seasons), were selected from the image dataset (as described in Section 2.2) using a crop classification map from Hengshui City for the year of 2017.

Two fields were sown on single cropping season with cotton and spring corn, and the third field was sown on double cropping season with winter wheat and spring corn. Daily NDVI-time-series images containing only pixels from each field were built at the original

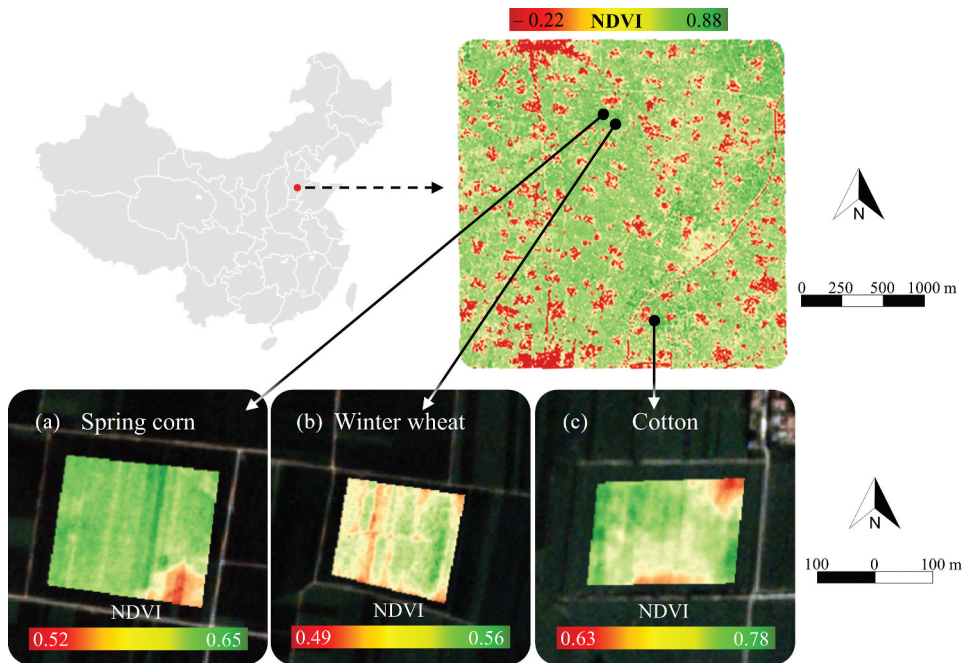


Figure 1. Location and area covered by the NDVI image from planet CubeSat at 218 DOY and detail of the cotton, spring corn and winter wheat fields at the maximum average NDVI across 2017 time-series (226, 229 and 110 DOY, respectively). NDVI images from cotton (a), spring corn (b) and winter wheat (c) fields were overlapped on an RGB image from 218 DOY.

spatial resolution (3 m). Thus, pixels from adjacent fields did not interfere in the pixel resize procedure, as described in Section 2.3.

The three selected fields (containing cotton, spring corn and winter wheat crops) represent the major crops in the studied area and their cropping patterns (single and double cropping seasons) and constitute the reality of cropland size in China. Hence, these fields are fragmented into small and narrow stripes of crop rows (defined in this paper as parcel), which lead to variability in sowing date and crop phenology within each field, as observed in Figure 1.

Figure 2 presents the monthly weather data (total rainfall and average maximum and minimum air temperature) from Hengshui City for the year of 2017. Although weather data is not available for each monitored field (which could provide further interpretation about how weather data is driving crop development and affecting the NDVI time-series) this information is important to subsidize the understanding the crop development according the agronomic requirements of water supply and temperature.

2.2. Planet CubeSat images acquisition and processing

Daily CubeSat scenes from 2017, on the Hengshui City, were acquired at the analytic product level, in which images had been orthorectified, the radiometric data represents the surface reflectance with a 16-bit depth and the positional accuracy is higher than 10 m. Each scene covers an area of approximately 20×20 km and, since the studied area is

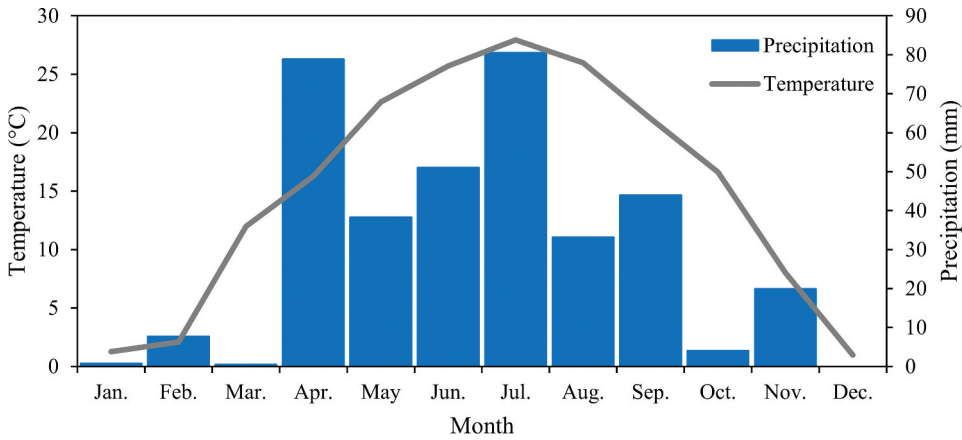


Figure 2. Monthly weather data (total rainfall and average air temperature) from Hengshui City, Hebei Province, China, for the year of 2017.

located within the same scene, there was no need for mosaicking process. The ground sampling distance at nadir on the obtained images is 3 m.

Planet CubeSat images are recorded on a 6600 × 4400 pixels CCD array (Aldeghi et al. 2019), which acquires both visible and near-infrared wavelengths. The bandwidths of the Planet CubeSat image are: 455–515 nm (blue), 500–590 nm (green), 590–670 (red) and 780–860 nm (near-infrared) (Maciel et al. 2020).

Only CubeSat scenes with more than 50% of cloud free pixels were acquired. Therefore, all the 119 available images for the year of 2017 were automatically converted into NDVI (Rouse et al. 1974). The distribution of the analysed Planet CubeSat scenes across 2017 is presented in Figure 3.

2.2.1. Reconstructing and smoothing NDVI-time-series

A recurrent challenge when using satellite data, especially time-series vegetation index, is to perform the gap-filling and to remove the effects of atmospheric condition on the obtained surface reflectance response. Those interferences are often provoked by the presence of undetected sub-pixel clouds, atmospheric dust, aerosols and gaseous absorbers (Atkinson et al. 2012).

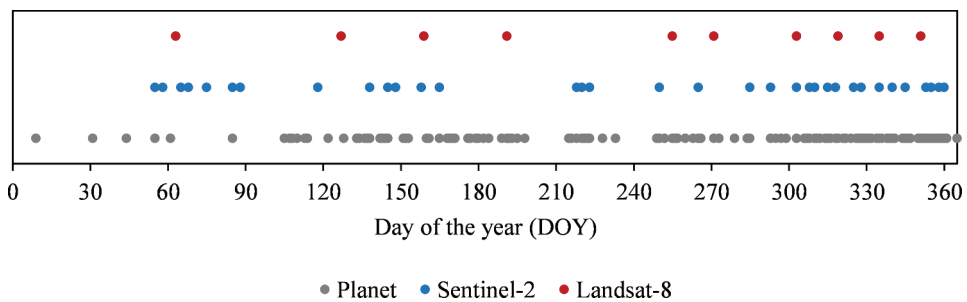


Figure 3. Distribution of available planet, Sentinel-2 and Landsat-8 images across 2017.

Hence, to the obtainment of daily time-series and to remove the influence of noise, better reflecting the internal behaviour of the crop growth curve, gap-filling and smooth algorithms are required. However, there are divergent recommendations regarding the choice of the gap-filling and smoothing method for each satellite product and application purpose, demonstrating that their accuracy is deeply related to the location of the target area and the vegetation characteristics (Atkinson et al. 2012; Qiu, Feng, and Tang 2016; Zhou et al. 2016).

In this context, after removing cloud pixels, the harmonic analysis of time series (HANTS) algorithm was applied to obtain a smoothed gap-free time series, removing further noises and maintaining the Planet CubeSat data consistency. The HANTS algorithm interpolates time series values by a Fourier transform and least squares method to obtain a new and smoother time series (Dong et al. 2019). According to Liang et al. (2017), NDVI time series, which has a strong seasonal dynamic, can be expressed using periodic series of low-frequency sine or cosine functions with different phases, frequencies, and amplitudes. HANTS algorithm is considered one of the most time-honoured methods to process satellite observed time series (Zhou, Jia, and Menenti 2015). The HANTS algorithm was applied through the IDL (Interactive Data Language) environment, allowing the acquisition of gap-free daily NDVI-time-series, containing 365 straight days, at 3 m spatial resolution.

2.3. Generating NDVI-time-series images at different spatial and temporal resolutions

Six NDVI-time-series images containing different temporal and spatial resolutions were generated, as described on Table 1.

The NDVI-time-series, after the daily reconstruction and smooth processing, named from now on as ‘daily NDVI- time-series’ image, were resized to 9 m and 30 m resolution using the ‘Resize Data Tool’ by pixel aggregate (average pixels’ value) from ENVI (Environment for Visualizing Images) software, resulting into three daily NDVI-time-series images with different spatial resolution. The reason the original 3 m resolution image was resized to 9 and 30 m resolutions is to analyse images with similar spatial resolution to Sentinel-2 Multi-Spectral Instrument – MSI (10 m), Landsat 7 Enhanced Thematic Mapper Plus – ETM+ – and Landsat 8 Operational Land Imager – OLI (30 m).

After that, the daily NDVI-time-series image (after the reconstructing and smoothing process, containing 365 straight days) were resampled to 4, 8 and 16 days intervals (NDVI daily values selected systematically at equal intervals), resulting in four NDVI-time-series images with different temporal resolution. Hence, besides the daily NDVI-time-series images (daily temporal resolution and 3 m spatial resolution), two daily NDVI-time-

Table 1. Description of the evaluated NDVI-time-series images.

NDVI-time-series image	Temporal resolution	Spatial resolution
Daily NDVI-time-series	Daily	3 m
9 m NDVI-time-series	Daily	9 m
30 m NDVI-time-series	Daily	30 m
4 days-NDVI-time-series	4 days interval	3 m
8 days-NDVI-time-series	8 days interval	3 m
16 days-NDVI-time-series	16 days interval	3 m

series image were evaluated at different spatial resolutions and three NDVI-time-series images were evaluated at different temporal resolution, resulting in six NDVI-time-series images for each crop field.

To evaluate the impact of different revisiting interval on satellite-based image acquisition and the delivered NDVI trajectory across the year, NDVI values from the daily time-series were extracted at the corresponding days of the 119 original images from Planet CubeSat. After that, the NDVI trajectory across the year was compiled at 4, 8, 16 and 32 days intervals of revisiting time.

Since the 119 available images were not equally distributed across the year, at some revisiting periods no image was available and at some revisiting periods more than one image was available. Hence, the image closest to the central day of each revisiting interval was selected to compose the NDVI trajectory across the year on each revisiting interval. The number of NDVI values at each revisiting interval across the year was: 61 (4 days interval), 37 (8 days interval), 22 (16 days interval) and 12 (32 days interval – this temporal resolution image is not described on [Table 1](#) since it was only used for the investigation of the impact of revisiting interval on NDVI trajectory across the year).

2.4. Data analysis

To assess the effect of the temporal and spatial resolutions on detecting within field variability, the NDVI profile (time-series) from all pixels from each field were extracted from all NDVI-time-series images ([Table 1](#)) and evaluated by their minimum, maximum, average, coefficient of variation and standard deviation across the year. The daily increase rate across time-series, expressed in percentage in relation to the NDVI value from the previous day (according to the temporal resolution of each NDVI-time-series image), was also evaluated. Besides that, the NDVI-time-series from Planet CubeSat was compared to the original time-series from Sentinel-2 and Landsat-8 over the study area for the same period. Only cloud free Sentinel and Landsat scenes were used and the available images across 2017 are presented in [Figure 3](#). Across 2017, original NDVI images from Planet, Sentinel-2 and Landsat-8 were available, at the same day, on 303 DOY (Day of the year) and 335 DOY.

The Principal Component Analysis (PCA) and Stepwise procedures were applied to select optimum features (days across the year) to assist the NDVI-time-series interpretation. Performed by the Unscrambler X software, version 10.4 (Camo Analytics), the PCA was applied to check whether the variance among the daily NDVI-time-series for each crop type ([Table 1](#)) can be explained (assessed by the cumulative variance of the first three principal components) and which dates across the year were more suitable for the time-series grouping (assessed by the loading correlation of each principal components).

PCA is a widely used data mining method that reduces the number of variables to be analysed (e.g. daily NDVI values across the year) and promotes, by a covariance matrix composed by all NDVI values across the year from all fields, the transformation of those variables into a new group of variables, called principal components – PC. Each principal component (PC) represents the linear combination of all analysed variables (NDVI time-series) to explain their variance and its score describes the percentage of variance that can be explained. The first principal component (PC1) carries most information of data variance, the second principal component (PC2) carries the residual information of PC1,

the third principal component (PC3) carries the residual information of PC2 and so on (Jolliffe and Cadima 2016; Li, He, and Fang 2007). The loading correlation of each PC, expressed in (r), is defined as the correlation of each variable (daily NDVI values across the year) with the principal component, and represents the contribution of each daily NDVI value to the PCA (Li, He, and Fang 2007; Holden and LeDrew 1998).

The stepwise procedure was carried out to select the NDVI values across the year that statistically group the analysed NDVI-time-series for each crop type, contributing to the time-series interpretation. In a forward and backward procedure, each variable (NDVI across the year) is added to or removed from a multilinear regression function, evaluated by the F -test and by the Wilks' Lambda value, following the likelihood principle (Karimi et al. 2005; Thenkabail et al. 2004; Draper and Smith 2014; Furlanetto 2018). The stepwise was carried out until no variable (with p -value < 0.05 – defined a priori) could be entered or removed from the function, as described by Furlanetto (2018). The selected NDVI values across the year were used to interpret the time-series.

To check the effect of temporal resolution on crop type grouping, 50 pixels were randomly selected and extracted from the daily, 4, 8 and 16 day-NDVI-time-series images (Table 1) using the region of interest (ROI) tool from ENVI software, assuring the sampling at the same geographical position in each field and each time-series image and submitted to PCA. The pixel selection was performed addressing the variability on crop phenology within each field, selecting pixels from all parcels.

To evaluate the impact of different revisiting times on NDVI trajectory across the year, the NDVI trajectory from all pixels from each field were extracted from the 4, 8, 16 and 32 days revisiting interval as well from the 119 available NDVI images.

3. Results

3.1. 3 m daily NDVI-time-series analysis

The daily NDVI time-series at 3 m spatial resolution of the single-season cotton and spring corn fields and of the double-season winter wheat and spring corn field are represented in Figure 4.

The obtained daily NDVI-time-series at 3 m spatial resolution (Figure 4) demonstrated to be singular for each field and to preserve the consistency of the original dataset. Table 2 displays the linear regression between NDVI values from the original dataset and after the HANTS algorithm.

Across the first 140 days of the year (DOY) it is possible to observe a large difference of NDVI between winter wheat and the other evaluated crops, especially between 100 DOY and 120 DOY, near the maximum NDVI of winter wheat crop (0.528 at 110 DOY). The peak of NDVI values on the time-series corresponds to the development status of winter wheat crop. During this period, the NDVI values from single crop fields demonstrated a flat shape, around 0.10 and without large variations across time. The beginning of cotton and single-season spring corn cropping seasons can be clearly identified by the increase of NDVI around 150 DOY. The beginning of spring corn cropping season at the double-season field demonstrated to be latter compared to the single-season field.

The peak of NDVI on cotton field (0.730 at 226 DOY) was superior compared to the single-season spring corn (0.617 at 229 DOY) and double-seasons spring corn (0.671 at

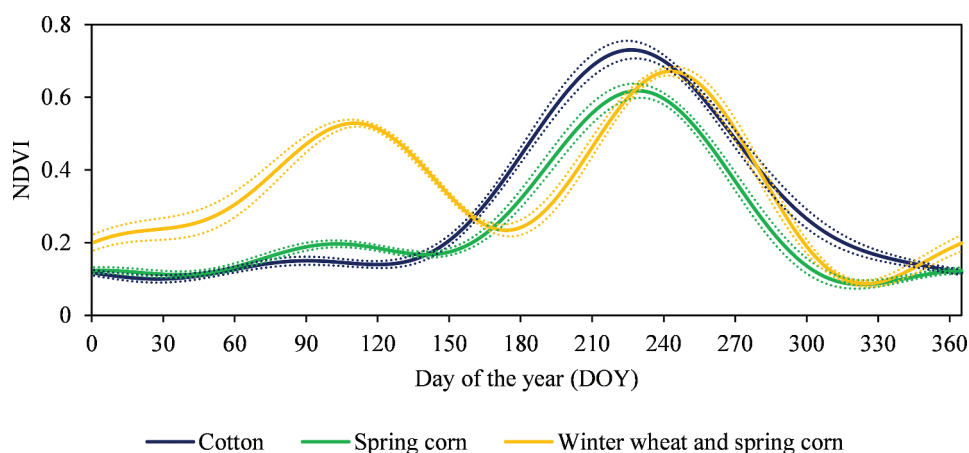


Figure 4. 3 m daily-NDVI-time-series of cotton, spring corn and winter wheat and spring corn fields. Coloured dots represent the limits of standard deviation for each field.

Table 2. Linear regression between NDVI from original dataset and after the HANTS algorithm.

Field	r	R^2	Slope	Intercept	RMSE
Cotton	0.990	0.981	0.940	0.020	0.030
Spring corn	0.988	0.977	0.939	0.005	0.029
Winter wheat and spring corn	0.976	0.953	0.953	0.003	0.042

*RMSE: root mean square error.

243 DOY). The end of cotton and spring corn seasons (both at single and double-season fields) can be also observed by the lowest NDVI values around 310 DOY.

According to Cui et al. (2020), the phenology assessment is crucial to understand vegetation relations. Furthermore, the use of NDVI- time-series has been recognized to be efficient to evaluate the dynamic of agricultural systems, especially when single and double-season fields present NDVI curves with different shapes (Bellón et al. 2017).

Masialeti, Egbert, and Wardlow (2010) monitored NDVI-time-series from major crops in Kansas, United States, and performed a deep description of NDVI-time-series shapes, considering phenological phases of positive and negative NDVI increment and peaks among crop types. As reported by Hill and Donald (2003), crop phenology might present differences among production areas. Liu et al. (2013) stated that environmental conditions, such as climatic factors (temperature, photoperiod, sunshine hours, solar radiation and precipitation), influence crop growth and phenology. In the same context, Wardlow, Egbert, and Kastens (2007) described the variability in time-series within crop type to be related to climatological conditions, agronomic management and sowing date.

Figure 5 presents the NDVI daily increase rate across the time-series of the evaluated fields. The knowledge of NDVI daily increase rate has been rarely reported by other research papers and has significant importance in the monitoring of crop conditions, providing deeper information of crop development across time.

During cotton crop development, the NDVI daily increase rate demonstrated a positive peak at 161 DOY (2.71%) and negative peak at 291 DOY (−2.07%). The spring corn fields presented, both at the single and double cropping season fields, positive daily increase

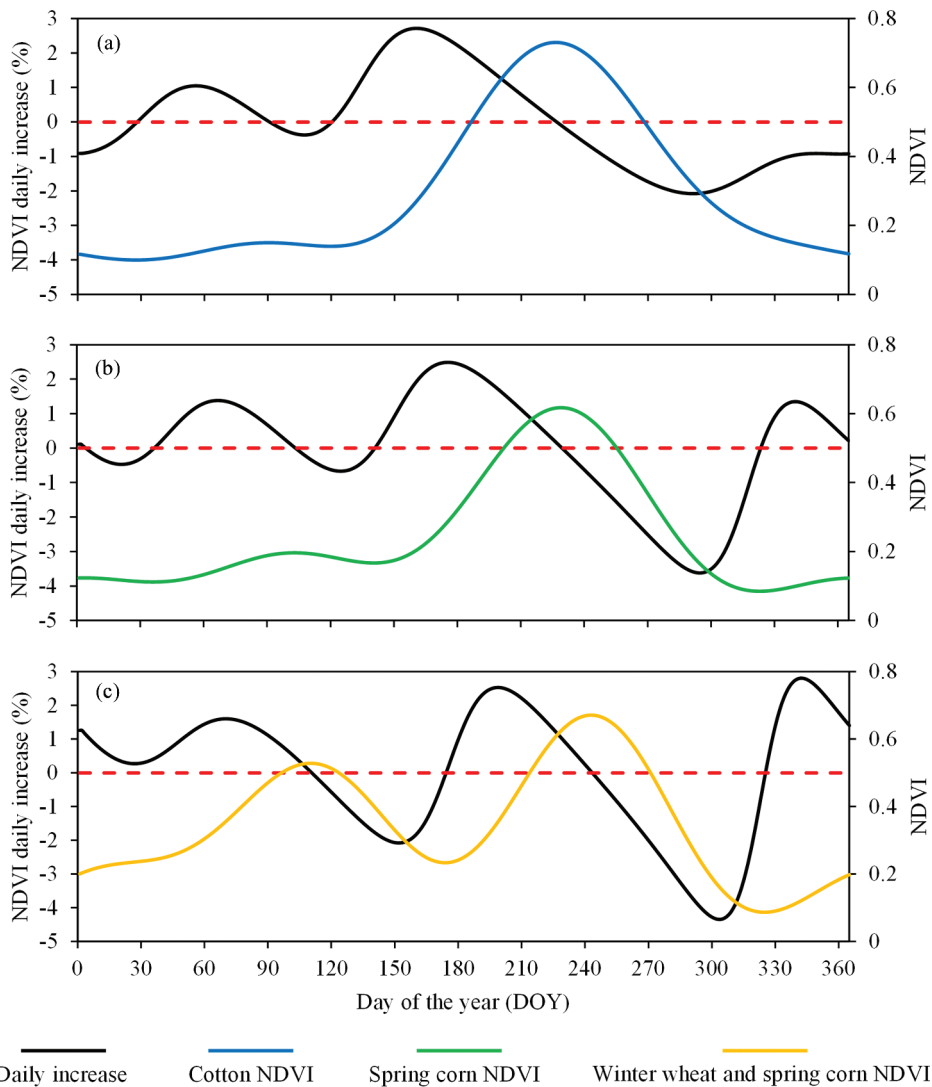


Figure 5. Daily increase (%) on cotton (a), spring corn (b) and winter wheat and spring corn (c) NDVI-time-series. The dashed red lines represent the limit between positive and negative increase.

rate at the beginning of cropping season similar to cotton field: 2.48% (176 DOY – single-season) and 2.52% (199 DOY – double-season).

However, the negative peak at the ending of spring corn cropping season demonstrated larger magnitude than the cotton field. The negative daily increase rate at the single-season field was -3.62% (295 DOY) and at the double-season field -4.34% (304 DOY).

Regarding winter wheat cropping season, the positive daily increase rate demonstrated a peak at 70 DOY (1.60%) and a negative peak at 152 DOY (-2.08%). As expected, in all fields and crops evaluated, the rate of null daily increase occurred on the same days when NDVI values reached the maximum values across the cropping season.

It is important to emphasize the magnitude between the maximum positive and negative daily increase rate of NDVI across the time-series. The lowest difference between positive and negative daily increase rate was observed for winter wheat crop: 3.68%, ranging from 1.60% to -2.08% . The cotton crop demonstrated intermediate difference between positive and negative daily increase rate: 4.78%, ranging from 2.71% to -2.07% . The largest magnitude of the difference between positive and negative daily increase rate was found in spring corn fields: 6.1%, ranging from 2.48% to -3.62% (single-season field) and 6.86%, ranging from 2.52% to -4.34% (double-season field).

3.2. Optimum NDVI features for NDVI time-series interpretation

The differences among NDVI time-series are corroborated by the PCA, where the first principal component explained 84% of data variance and the second principal component explained 14% of data variance. According to Wang (1999), when principal components reach over 80%, the remaining components can be omitted in further analysis.

Figure 6 presents the loading correlation of the first and second principal components and the coefficient of determination (R^2) of the selected bands on the stepwise procedure.

The first principal component demonstrated a higher grouping power, with loading correlation over 0.9 in the first 140 days of the year and around 195 DOY, discriminating the double-seasons field from single-season fields. The first 140 days of the year correspond to the winter wheat cropping season, as described on Figures 4 and 6. The 195 DOY corresponds: to the positive slope on NDVI values on cotton and spring corn (single-season) fields; and to the later increase of NDVI in the double-season spring corn field.

The second principal component demonstrated high effectiveness on grouping cotton from spring corn (single-season) time-series. Hence, three peaks of loading correlation were detected at 162 DOY, 239 DOY and 293 DOY. The 162 DOY represents the ending of winter wheat season and the positive slope at the beginning of cotton and spring corn (single-season) fields, while the 239 DOY corresponds to the moment close to the peak of

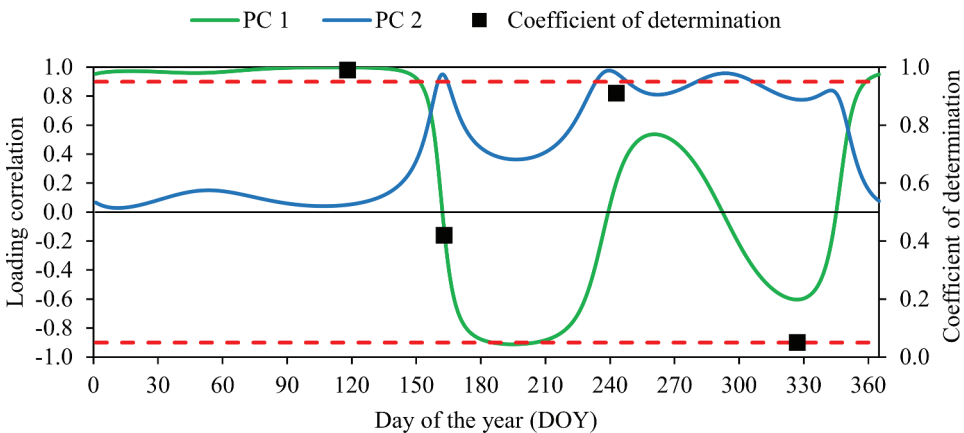


Figure 6. Loading correlations of the principal component analysis (PCA) and coefficient of determination (R^2) of the selected bands on the stepwise procedure. Dashed red lines represent the 0.9- and -0.9 line of loading correlation.

spring corn at the double-season field and negative slope of cotton and spring corn at single-season field. The 293 DOY is represented by a large negative increase rate of spring corn NDVI (-3.61 and -3.88 at the single and double-season fields respectively) simultaneously to a lower negative increase rate of cotton NDVI (-2.07), which is corroborated to the NDVI daily increase, as presented in [Figure 5](#).

The results obtained on the PCA are in agreement to the results found on the stepwise procedure, in which the NDVI daily values for crop type grouping were selected ([Figure 6](#)). The NDVI at 118 DOY was found to be the best NDVI to group the evaluated time-series, with $R^2 = 0.99$. This date corresponds to the moment close to the NDVI peak of winter wheat crop while the others two fields remained non-cultivated, with low values of NDVI. The second best NDVI to group the NDVI-time-series was found at 163 DOY, with $R^2 = 0.91$. The 163 DOY is just one day from the 162 DOY, which, as described on the PCA, represents the ending of winter wheat season and the positive slope at the beginning of cotton and spring corn (single-season) fields.

The selected NDVI at 243 DOY demonstrates a coefficient of determination equal to 0.42. The 243 DOY is just 4 days distant from the 239 DOY, which, as described on the PCA, corresponds to the moment close to the peak of spring corn at the double-season field and the beginning of the negative slope of cotton and spring corn at single-season field.

The NDVI at 327 DOY was selected with $R^2 = 0.05$, the lowest among the selected daily NDVI values. This date represents the minimum values of NDVI on corn fields (both at single and double-seasons) while the NDVI in the cotton fields was still decreasing, as shown in [Figure 4](#).

According to [Zeng et al. \(2020\)](#), wavelet selection is one of the most used methods for data transformation to characterize the phenology of vegetation from satellite observations; and the PCA has been recognized to be efficient in detecting seasonal changings in time-series. [Bellón et al. \(2017\)](#), stated that the first principal component carries the information of major variability among crop types and the second principal component carries the information of intra-seasonal variability. Similarly, we found the first PC to be related to the winter wheat cropping season (when the other fields remained unsown) and the second PC to be related to the intra-seasonal variability between cotton and spring corn.

The use of optimum NDVI features for crop monitoring plays a role in spectral data reduction without losing spectral information. According to [Peña and Brenning \(2015\)](#), spectral features selection can be carried out for the best-performing classifier and feature set in order to determine whether a reduced number of image dates can achieve competitive results. [Zhou, Zhang, and Townley-Smith \(2013\)](#) observed that a reduction in time-series length and spectral bands reduced 75% of the data volume and led to a decrease of only 2% in the accuracy. Thus, considering the possibility of developing a classification model based on NDVI features from a specific year and its application on future cropping seasons ([Masiale, Egbert, and Wardlow 2010](#)), we emphasize the potential of selecting optimum features from daily NDVI time-series to assist the crop type monitoring at local and regional levels, taking into account the crop development variation due to sowing dates, climatological condition and management practices.

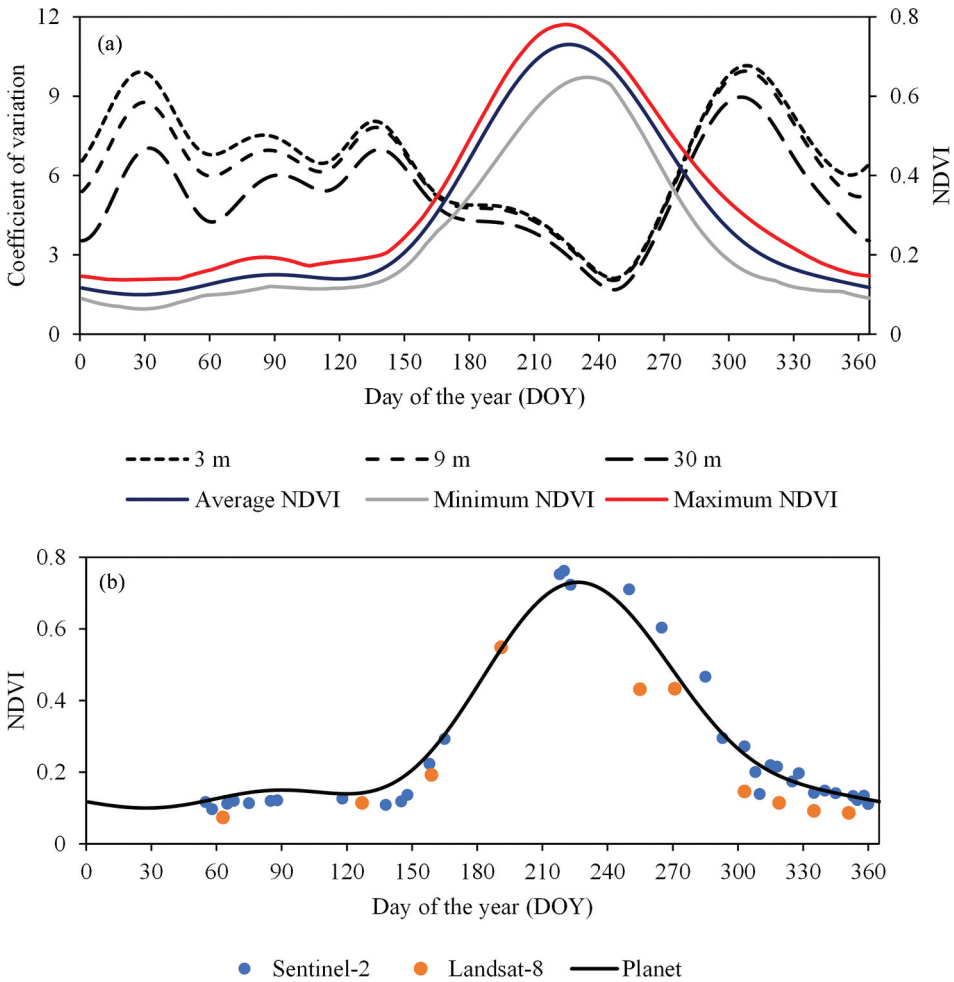


Figure 7. Coefficient of variation (%) in the cotton field at 3 m resolution, 9 m resolution and 30 m resolution and minimum, maximum and average NDVI at 3 m resolution across time-series (a) and NDVI-time-series from Planet, Sentinel-2 and Landsat-8 (b).

3.3. Impact of spatial resolution on within field monitoring

3.3.1. Cotton

Figure 7(a) displays the coefficient of variation in the cotton field at 3 m resolution (10,004 pixels), 9 m resolution (1,107 pixels) and 30 m resolution (96 pixels) and the minimum, maximum and average NDVI at 3 m resolution across the year. The NDVI-time-series from Planet at 3 m resolution and from original Sentinel-2 and Landsat-8 images are presented in Figure 7(b).

Across the entire time-series, higher coefficients of variation were observed on the 3 m resolution image. It is possible to observe two peaks of coefficient of variation across cotton cropping season: one at the beginning of the year (28 DOY), which probably occurred due to secondary field management and small fractions of different types of vegetation in each parcel inside the field, and one at the end of NDVI negative increase

(308 DOY). Close to the maximum NDVI values (226 DOY) the coefficient of variation presented low values. The peaks of coefficient of variation in NDVI values are associated to differences in crop phenology from each parcel within the field. When the crop reaches the moment close to the maximum NDVI, the shape of the curve presents a plateau. Hence, at this moment the differences in crop NDVI within the field are minimized since all pixels are close to their maximum values, reducing the variability. Besides that, it is possible to observe that the NDVI derived from Planet, Sentinel-2 and Landsat-8 presented similar trend across the year.

Figure 8(a) presents the NDVI images from cotton field at 207 DOY, when the maximum standard deviation was observed, at 3 m, 9 m and 30 m resolution. The NDVI images derived from the original Planet, Sentinel-2 and Landsat-8 satellites at 303 DOY (when images from the three satellites were available) are presented in Figure 8(b). The narrower range between minimum and maximum NDVI associated with increasing pixel size can be observed among the three satellites. For Planet, NDVI ranged from 0.17 to 0.42, for Sentinel-2 from 0.18 to 0.36 and for Landsat-8 from 0.11 to 0.17.

3.3.2. Spring corn

Figure 9(a) displays the coefficient of variation in the spring corn field (single-season) at 3 m resolution (15,561 pixels), 9 m resolution (1,716 pixels) and 30 m resolution (156 pixels) and the minimum, maximum and average NDVI at 3 m resolution across the year. The NDVI time-series from Planet at 3 m resolution and from original Sentinel-2 and Landsat-8 images are presented in Figure 9(b).

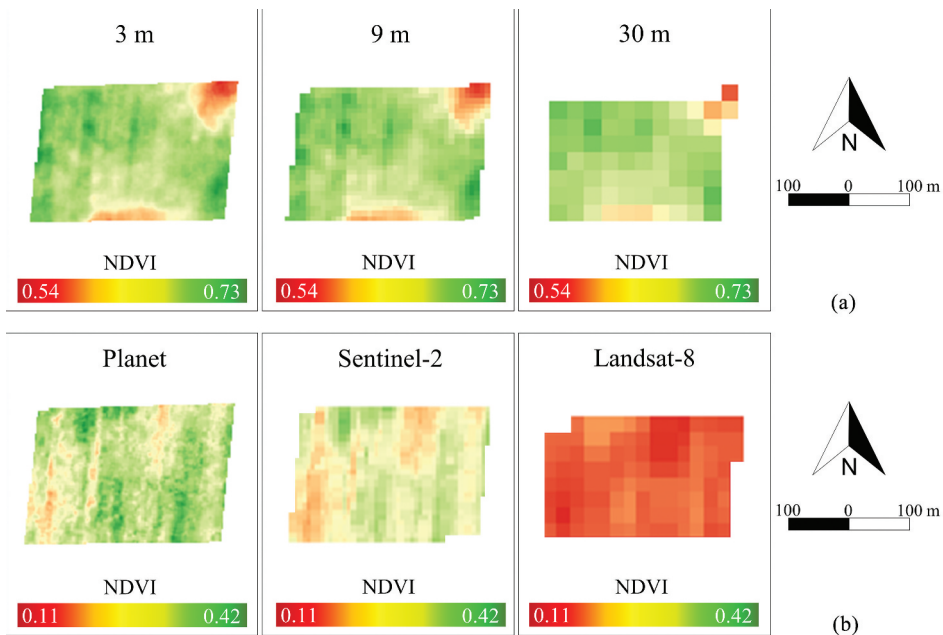


Figure 8. NDVI images from cotton field at 207 DOY at 3 m, 9 m and 30 m resolution (a) and NDVI images from planet, Sentinel-2 and Landsat-8 at 303 DOY (b).

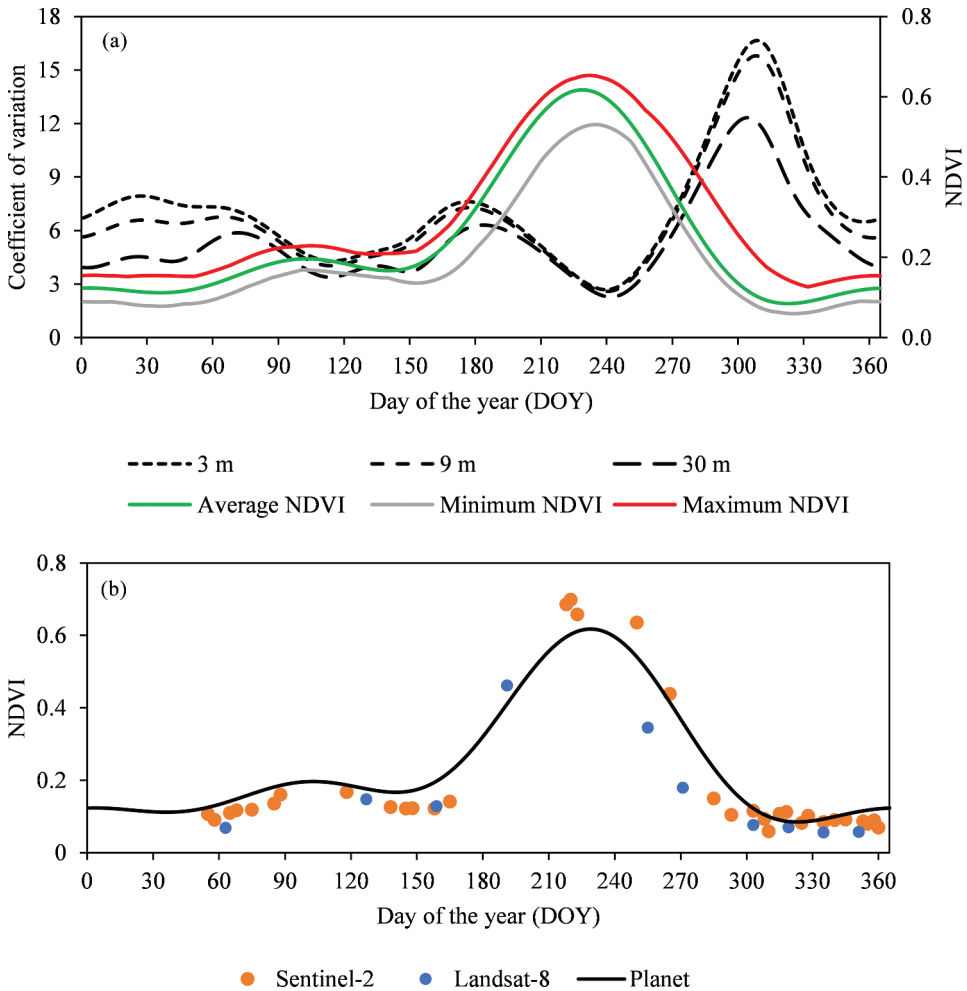


Figure 9. Coefficient of variation (%) in the spring corn field at 3 m resolution, 9 m resolution and 30 m resolution and minimum, maximum and average NDVI at 3 m resolution across time-series (a) and NDVI-time-series from Planet, Sentinel-2 and Landsat-8 (b).

As it has been observed in cotton field, the largest NDVI coefficient of variation in the spring corn (single-season) field were observed at the negative (309 DOY) slope of NDVI values across cropping season, and lower coefficient of variation was detected when crop reached the maximum NDVI value (229 DOY), demonstrating that when the crop reaches the moment close to the maximum NDVI, the shape of the curve presents a plateau, and at this moment, the variability in crop spectral response within the field is minimized. As observed for the cotton field, a similar trend across the year could be observed for the NDVI derived from Planet, Sentinel-2 and Landsat-8.

Figure 10 presents the NDVI images from spring corn field at 200 DOY, when the maximum standard deviation was observed, at 3 m, 9 m and 30 m resolution. The NDVI images derived from the original Planet, Sentinel-2 and Landsat-8 satellites at 303 DOY are presented in Figure 10(b). The narrower range between minimum and maximum NDVI associated with

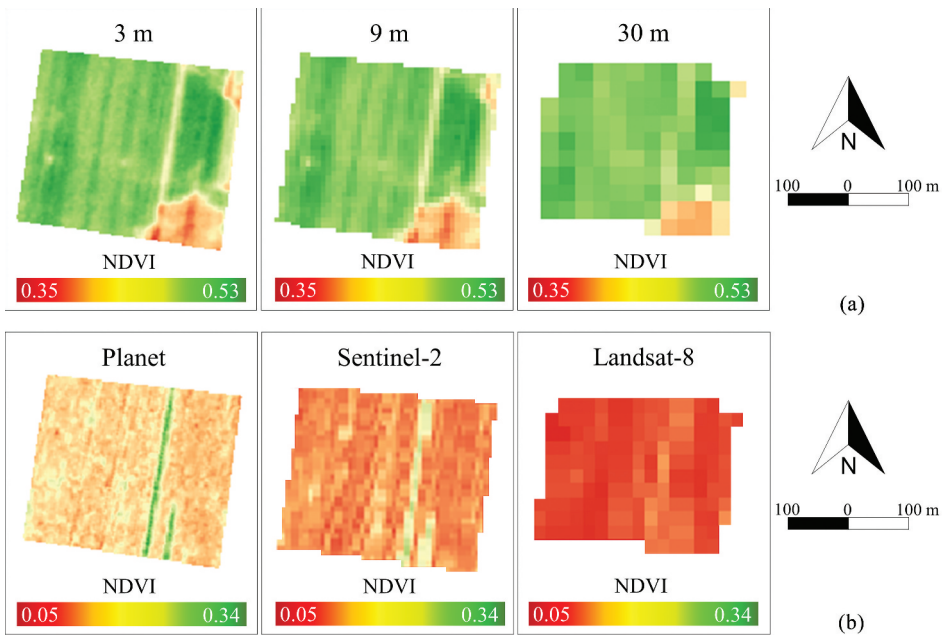


Figure 10. NDVI images from spring corn field at 200 DOY at 3 m, 9 m and 30 m resolution (a) and NDVI images from Planet, Sentinel-2 and Landsat-8 at 303 DOY (b).

increasing pixel size can be observed among the three satellites. For Planet, NDVI ranged from 0.08 to 0.34, for Sentinel-2 from 0.07 to 0.25 and for Landsat-8 from 0.05 to 0.11.

3.3.3. Winter wheat and spring corn

Figure 11(a) displays the coefficient of variation in the winter wheat and spring corn field (double-season) at 3 m resolution (9,991 pixels), 9 m resolution (1,088 pixels) and 30 m resolution (100 pixels) and the minimum, maximum and average NDVI at 3 m resolution across the year. The NDVI time-series from Planet at 3 m resolution and from original Sentinel-2 and Landsat-8 images are presented in Figure 11(b).

Four peaks of coefficient of variation were observed across time-series (Figure 11): at the beginning of winter wheat cropping season in 2017 (42 DOI) and 2018 (339 DOI); and at the beginning and ending of spring corn cropping season (188 DOI and 301 DOI, respectively). Following the results observed on the cotton and spring corn (single-season) fields, lower standard deviation was observed close to the peak of NDVI values both on wheat (110 DOY) and corn (243 DOY) seasons.

By the observed values of standard deviation around 150 DOY, the ending of winter wheat cropping season, demonstrated to be homogeneous within the field. The decrease in coefficient of variation according to the enlargement of pixel size could be observed both across winter wheat and spring corn seasons. The similar trend across the year for the NDVI derived from Planet, Sentinel-2 and Landsat-8 could be observed for the spring corn cropping season (from 180 DOY to 330 DOY) but not for the winter wheat cropping season (from 30 DOY to 180 DOY) most likely to the low number of available images across that period (Figure 3).

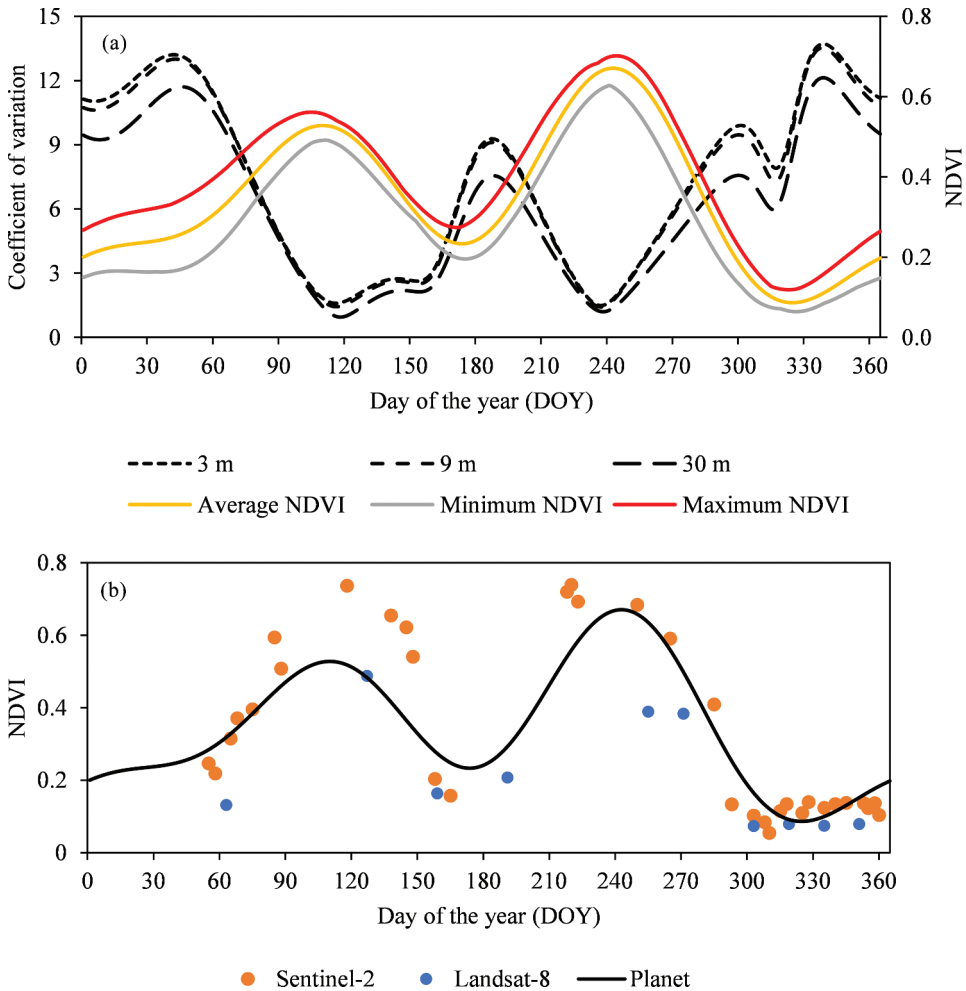


Figure 11. NDVI standard deviation in the winter wheat and spring corn field (double-season) at 3 m resolution, 9 m resolution and 30 m resolution and minimum, maximum and average NDVI at 3 m resolution across time-series (a) and NDVI-time-series from Planet, Sentinel-2 and Landsat-8 (b).

Figure 12 presents the NDVI images from winter wheat and spring corn field at 57 DOY, when the maximum standard deviation was observed, at 3 m, 9 m and 30 m resolution. The NDVI images derived from the original Planet, Sentinel-2 and Landsat-8 satellites at 303 DOY are presented in Figure 12(b). The narrower range between minimum and maximum NDVI associated with increasing pixel size can be observed among the three satellites. For Planet, NDVI ranged from 0.07 to 0.25, for Sentinel-2 from 0.07 to 0.20 and for Landsat-8 from 0.06 to 0.12.

Planet CubeSat images provided well detailed pixels capable of detecting larger variability within each studied crop compared to medium spatial resolution images, especially at 30 m resolution, demonstrating that small pixel leads to a higher detection of within field variability. It was also found (data not shown) that at lower spatial resolutions the minimum values of NDVI are increased and the maximum values are

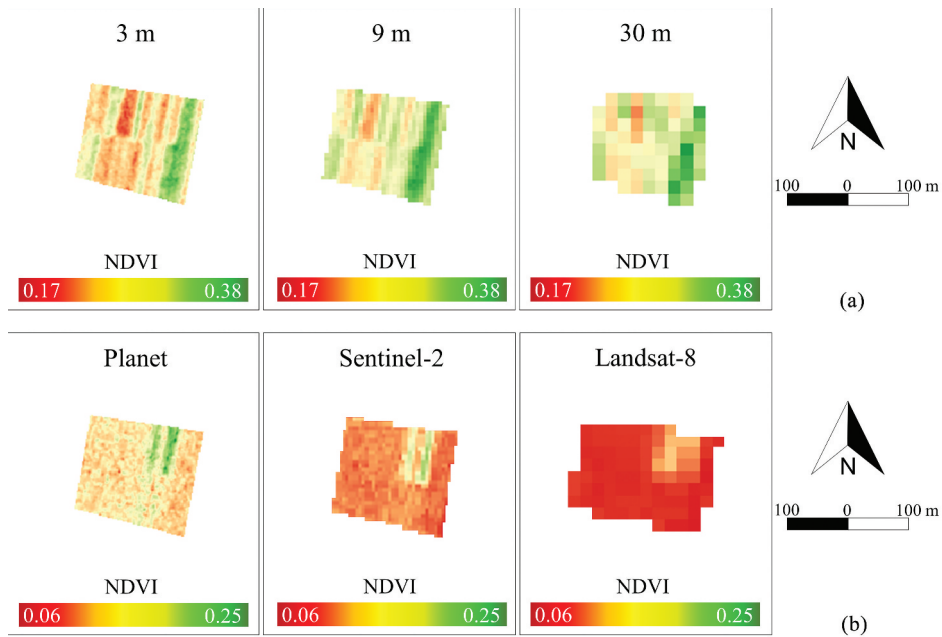


Figure 12. NDVI images from winter wheat and spring corn field at 57 DOY at 3 m, 9 m and 30 m resolution (a) and NDVI images from planet, Sentinel-2 and Landsat-8 at 303 DOY (b).

decreased, compromising the range of values detected within the same field. These effects might be especially important if low spectral variability is observed during key phenological phases for crop management. In this scenario, the variability observed within agricultural areas is mostly due to: differences in sowing date of each parcel (narrow stripes of crop rows), which created variability in crop phenology; and to differences in agronomical practices. Thus, the use of high temporal and spatial resolution images might contribute to detect slight changes in crop development and phenology in short time intervals and a larger number of pure pixels can be obtained even in small agricultural areas, minimizing the pixel mixing that might lead to misinterpretation of surface reflectance variability.

The impact of spatial resolution on crop monitoring by means of remote sensing has been reported for over twenty years (Pax-Lenney and Woodcock 1997). However, most of previous studies used coarser resolutions from Sentinel-2 Multi-Spectral Instrument – MSI, Landsat 7 Enhanced Thematic Mapper Plus – ETM+ – and Landsat 8 Operational Land Imager – OLI Löw and Duveiller (2014) investigated the optimum pixel size for monitoring crop systems in different landscapes and found that none spatial resolution fits all applications. According to the authors, the mixed pixels represent the largest effect of spatial resolution on crop classification, affecting the pixels' purity. Thus, the larger the pixel size, the larger the mixed pixels, demonstrating that each landscape and crop type might be affected in different proportions. Vrieling et al. (2017) evaluated the effect of spatial resolution on spectral variability within a highly dynamic eco-system using 10, 30 and 100 m spatial resolution images and concluded that most detailed features can be assessed when higher spatial resolution images are used. Comparing the Planet CubeSat

to Sentinel-2 and Landsat 8 images in the prediction of forest canopy height, Shimizu et al. (2020) point out the highest accuracy obtained for Planet CubeSat images.

3.4. Impact of temporal resolution on crop monitoring

3.4.1. NDVI trajectory across the year

Figure 13 presents the average NDVI trajectory (submitted to smooth process via HANTS algorithm without filling the missing values between each pair of NDVI images) across time-series on cotton (a), spring corn (b) and winter wheat and spring corn (c) fields using all 119 available Planet CubeSat images and at daily, 4, 8, 16 and 32 days revisiting intervals.

On the cotton and spring corn fields (Figure 13(a,b)) it is possible to observe that the NDVI trajectory across time-series is less affect during periods when the fields remain unsown (e.g. during the first 120 DOY). However, during periods when the NDVI time-series is driven by the crop development (e.g. cotton, spring corn and winter wheat) differences in NDVI trajectory can be observed.

For the three evaluated fields, the use of all available Planet CubeSat images or their evaluation at 4, and 8 days revisiting intervals (119, 61 and 37 images across time-series respectively) did not result in large differences in NDVI trajectory across time-series. At 16 days revisiting intervals (using 22 images across time-series) the NDVI trajectory demonstrated to be slightly different from the trajectory observed at shorter revisiting intervals. However, at 32 days revisiting intervals, using only 12 images across time-series, well-marked differences can be observed in NDVI trajectory on the three evaluated fields.

The well-marked differences in NDVI trajectory at 32 days revisiting time can be observed on the base of the slope at the beginning of cotton and spring corn (both at single and double cropping season) fields and at both sides of the shoulder of NDVI plateau of the three evaluated crops, diminishing the amount of spectral information available for each pixel across time-series.

Cui et al. (2020) evaluated crop phenology under different temporal resolution and reported that the detection of detailed temporal dynamics of vegetation is undermined as the temporal resolution increases. The authors also stated that larger influences in crop monitoring were observed in temporal resolutions larger than 18 days. Straw and Henry (2018) demonstrated that the larger the interval between images within time-series, the smaller the range of NDVI values detected within the same area, expressed by the increase of minimum values and decrease of maximum values.

3.4.2. Spectral data dimensionality

The 2-D score plot of the PCA for NDVI-time-series is presented in Figure 14 at 3 m daily (a), 4 days (b), 8 days (c) and 16 days (d) intervals and at daily 9 (e) and 30 (f) m resolution. In all simulated temporal resolutions, the cumulative score of the first and second principal components reached 98%.

In accordance to the results previously discussed (Figure 6), the OCA was capable of grouping the three crop fields. The winter wheat and spring corn double-season field can be clearly identified in all 2-D score plots (blue dots) due to the NDVI time-series at the first 140 DOY, comprising the winter wheat crop (Figure 3) and highlighted by the loading correlation of the first principal component (Figure 6). The NDVI-time-series from corn

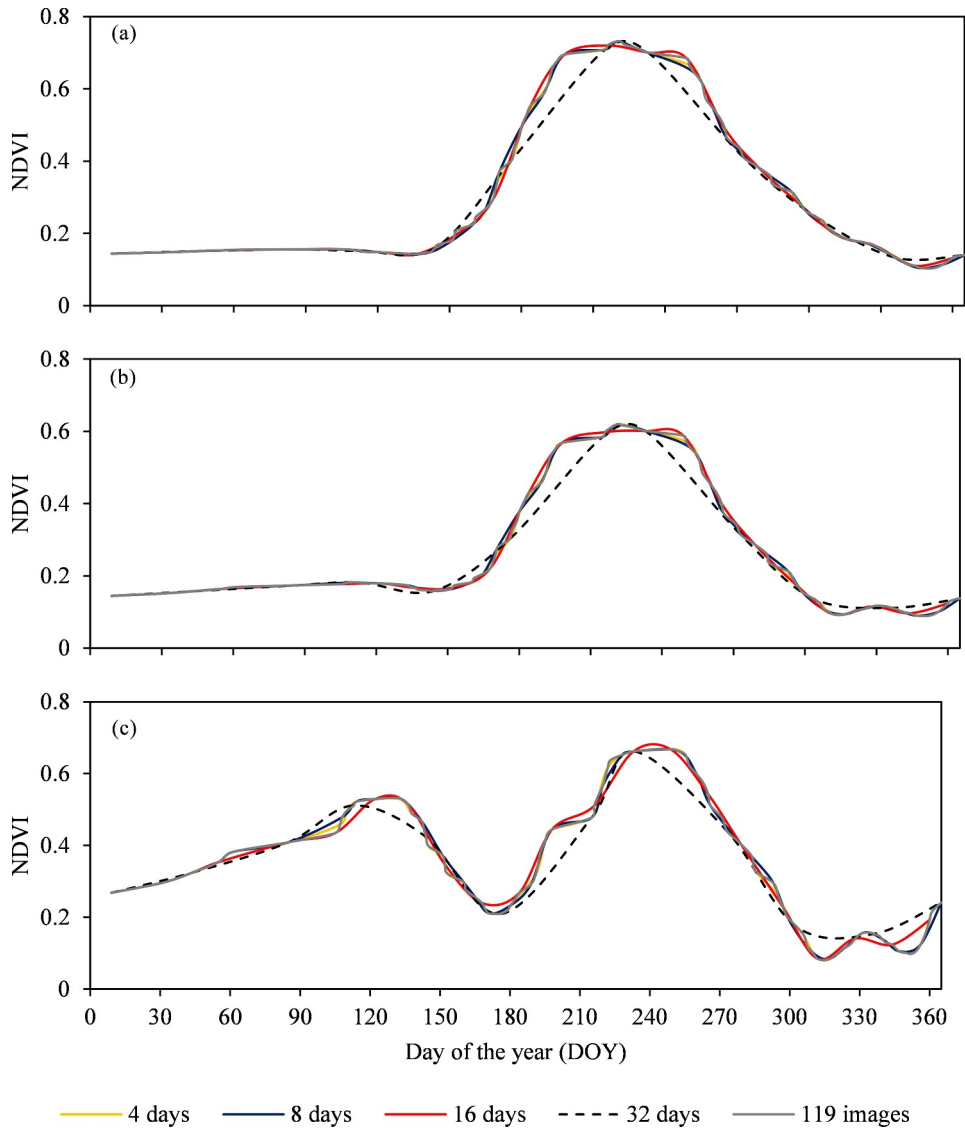


Figure 13. Average NDVI trajectory (submitted to smooth process via HANTS algorithm without filling the missing values between each pair of NDVI images) on cotton (a), spring corn (b) and winter wheat and spring corn (c) fields using all 119 available planet CubeSat images and at 4, 8, 16 and 32 revisiting intervals.

(single-season) and cotton fields presented similar shape but were well grouped between them in all simulated temporal resolutions (red and grey dots).

Although the crop fields could be consistently grouped regardless the simulated temporal and spatial resolution, the dimensional space among crop fields in the 2-D score plot between the first and second principal components demonstrated to be reduced as the interval on NDVI time-series increases. Hence, the smaller amount of

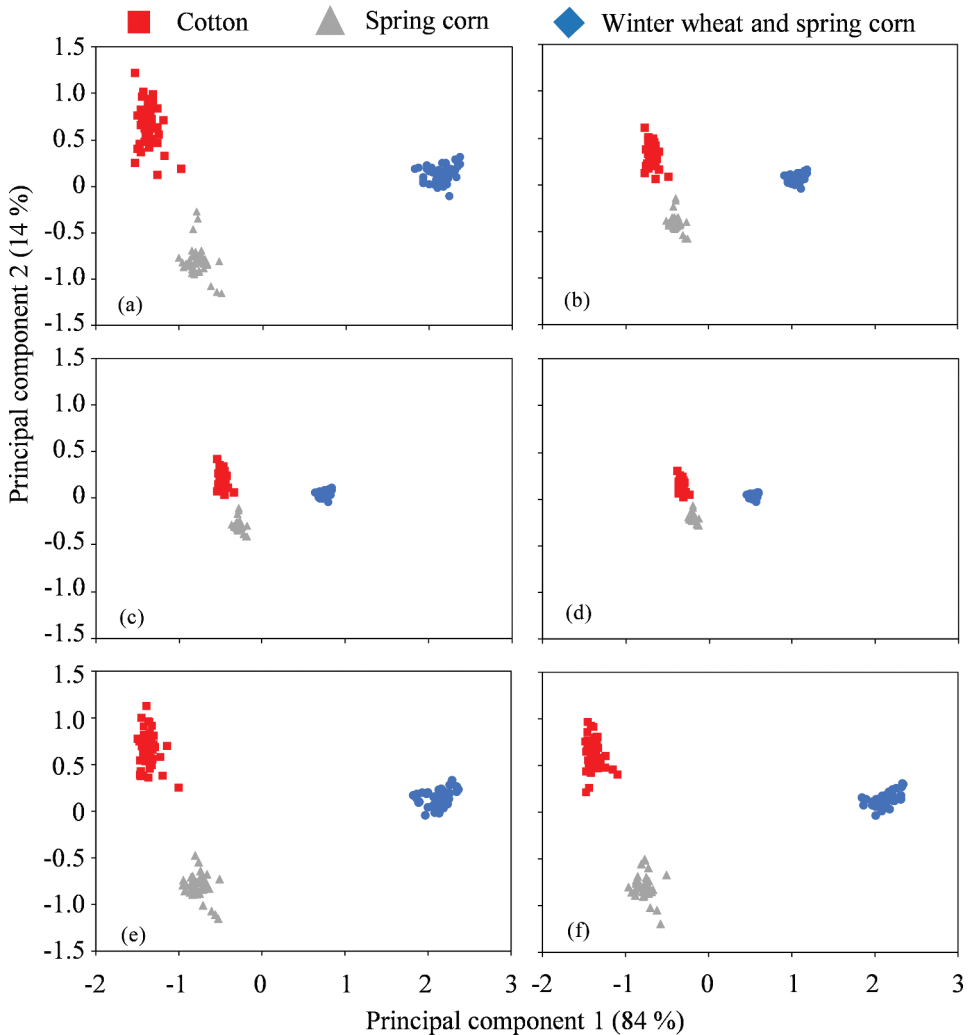


Figure 14. Principal component analysis for crop type at daily (a), 4 (b), 8 (c) and 16 (d) days NDVI-time-series at three m resolution and daily NDVI-time-series at 9 (e) and 30 (f) m resolution NDVI-time-series.

spectral information (NDVI values) across the year diminished the distance among crop types.

3.4.3. Increase rate

Figure 15 presents the increase rate (positive or negative) of NDVI time-series from cotton (a), spring corn (b) and winter wheat and spring corn (c) fields at daily temporal resolution and at 4 days, 8 days and 16 days temporal resolution. The enlargement of the temporal resolution deeply affected the increase rate of NDVI values between images from time-series. In all fields, the daily increase rate of NDVI (well detailed in Figure 5) demonstrated lower values compared to the 4, 8 and 16 days temporal resolutions.

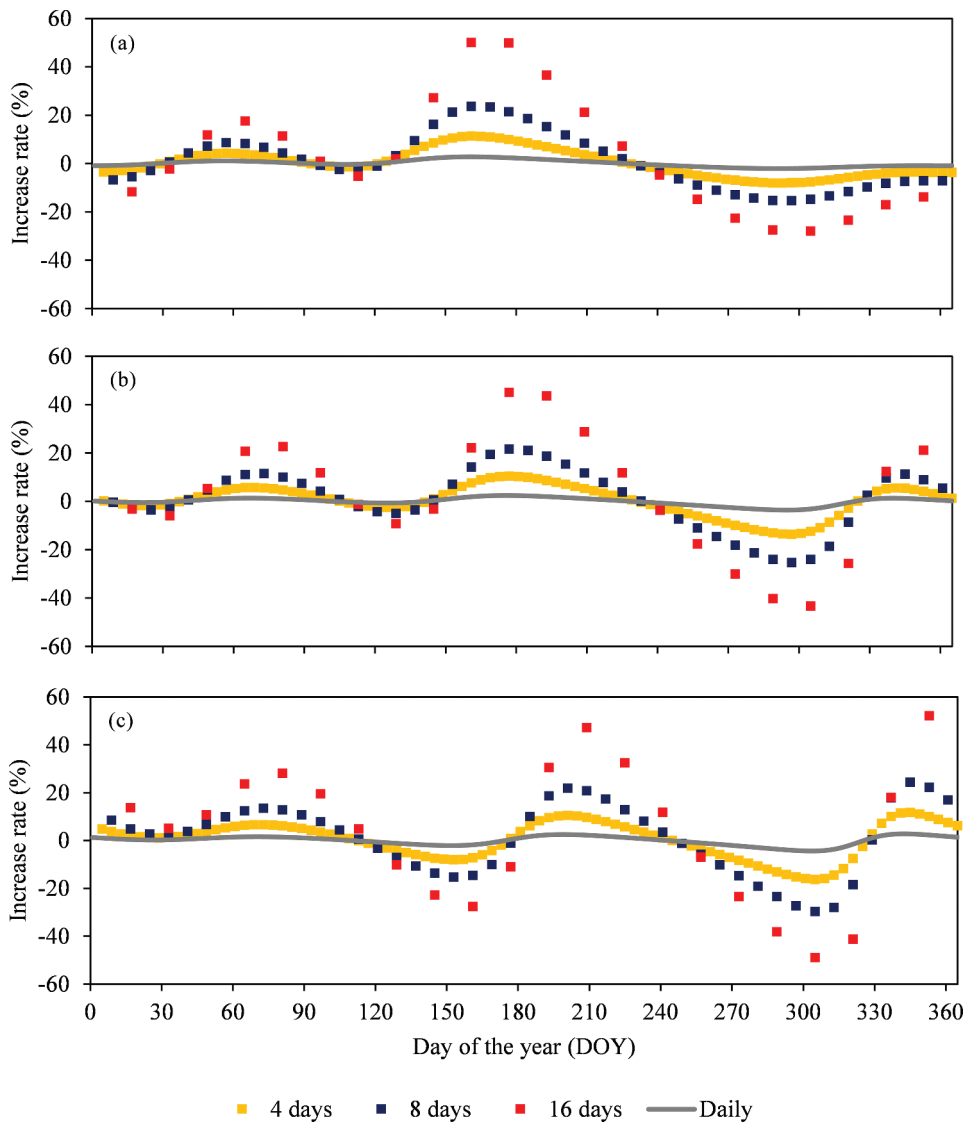


Figure 15. Increase rate (%) of NDVI from cotton (a), spring corn (b) and winter wheat and spring corn (c) fields at daily, 4, 8 and 16 days temporal resolution.

The differences in the increase rate according to temporal resolution are due to the cumulative rates in the interval between NDVI images. At daily NDVI-time-series, crop development information can be extracted in a more detailed level, detecting slight differences from one day to another. However, at larger temporal resolution, larger increase rates are detected, with abrupt changes in the crop spectral behaviour between NDVI images.

In the cotton field (Figure 15(a)), the NDVI increase rate at daily temporal resolution presented positive and negative peaks of 2.71% and -2.07% , respectively. These values demonstrated to be 11.30% and -8.05% at 4 days temporal resolution; 23.65% and

–15.39% at 8 days temporal resolution; and 50.03% and –27.89% at 16 days temporal resolution.

Similar results were obtained in the spring corn field (Figure 15(b)), when the positive and negative peaks of NDVI increase rate at daily temporal resolution shifted from 2.48% and –3.62%, respectively, to 10.31% and –13.69% (4 days temporal resolution), 21.52 and –25.41 (8 days temporal resolution) and 44.98% and –43.45% (16 days temporal resolution).

Regarding the winter wheat crop (Figure 15(c)), the positive and negative peaks of NDVI increase rate at daily temporal resolution (1.60% and –2.08%, respectively) demonstrated to be higher at larger intervals between images: 6.05% and –7.25% (4 days temporal resolution), 12.81% and –14.56% (8 days temporal resolution) and 28.02% and –27.61% (16 days temporal resolution).

Following the same trend, in the spring corn crop (Figure 15(c)), the positive and negative peaks of NDVI increase rate at daily temporal resolution (2.52% and –4.34%, respectively) showed higher values at 4 days temporal resolution (11.64% and –16.27%), at 8 days temporal resolution (24.39 and –29.64%), and at 16 days temporal resolution (52.07% and –48.86%).

The enlargement of positive and negative peaks of NDVI increase rate according to the temporal resolution is due to the cumulative rates in the interval between NDVI images and highlights the diminishment of spectral information on time-series, affecting the detection of small differences in crop development across time. At larger temporal intervals abrupt changes in crop development might be detected without knowing the intercurrent factors between images. At daily temporal resolution, slight differences in crop growth can be detected, enhancing the amount of spectral information for crop monitoring. Li and Roy (2017) analysed the revisit intervals of Landsat 8 and Sentinel-2 and its implications for terrestrial monitoring, demonstrating that at higher temporal resolution larger amount of spectral information is acquired.

3.5. Perspectives for planet CubeSat on crop monitoring

The importance of using high spatial and temporal resolution time-series is associated to the timing of occurrence of factors that might reduce crop yield and where control actions should be applied. For instance, the identification of plant disease, insect attack is crucial for time efficient decision making. In the other hand, the soil management and correction of fertility levels are deeply associated to the spatial variability in the agricultural area. If considered together, spatial and temporal resolutions play a role in the identification of variability within the crop system and in the definition of management zones, which is essential to explore the maximum yield potential in each area.

Considering both temporal and spatial resolution as key factors for crop monitoring (Liu et al. 2018, 2019) and the rapidly increasing availability of very high-resolution imagery, Planet CubeSat images still requires further assessments of its data and its application in crop investigations (Myers et al. 2019). Hence, exploring the high spatial resolution daily NDVI time-series from Planet CubeSat images can contribute for crop monitoring at small size areas and complex landscapes.

Three factors impose limitations to the present paper: the small number of evaluated fields, only one year of time-series and the absence of ground data regarding sowing

dates, management practices, phenological stages and yield. However, even under the limitations imposed by these three factors, this paper addressed the use of high spatial resolution daily NDVI time-series from Planet CubeSat images for crop monitoring, demonstrating the merit of the used remote sensed product in the identification of fine temporal and spatial variability in the studied area, which may contribute to better site-specific management of crop development in a time-efficient manner, assisting governmental and corporative decision make over technical issues, such as supply regulation, food security and financial market.

Based on the limitations and findings of this paper, it is important to describe the possibilities of using the Planet CubeSat NDVI-time-series in future research. In this context, the studied area shall be extended to a regional level, where it would be possible to understand the regional variability in the NDVI-time-series. Furthermore, the analysis of several years would improve the understanding of variability among cropping seasons. Besides that, the collection of ground data shall provide valuable information about crop development and, based on these information, spectral models could be developed aiming at predicting biophysical parameters of crop systems. Considering these perspectives, the use of robust statistical methods will be essential for better understand the relation between crop development and NDVI time-series.

4. Conclusions

This paper aimed to investigate the potential of using high spatial resolution daily NDVI time-series from Planet CubeSat images for crop monitoring. The obtained NDVI time-series from cotton, spring corn and winter wheat fields demonstrated to be well shaped and smooth.

The NDVI daily increase rate demonstrated to be useful to analyse slight changes on crop development in short periods of time. PCA and the stepwise procedure highlighted the best time across the year for NDVI time-series interpretation and grouping, demonstrating the potential of selecting NDVI features to develop spectral models that would assist the management of agricultural activities at local and regional levels.

The effect of spatial resolution was assessed by the ability of remote sensing data to detect within field variability. As the pixels size gets larger, the maximum NDVI values decrease, while the minimum NDVI values increase, shorting the range of NDVI and its coefficient of variation within each crop field. Hence, at high spatial resolution images (e.g. Planet CubeSat), well detailed pure pixels are capable of detecting larger variability within each crop field.

In the same way, the daily temporal resolution from Planet CubeSat images allowed the detection of slightly changes on crop development in a very short time interval. As the interval (days) between images gets larger, the changes in crop spectral response are detected at larger rates, without any spectral information of the intercurrent factors between one to another imagery date. Hence, the daily NDVI time-series from Planet CubeSat can lead to better understanding of crop development through time.

The high temporal and spatial resolutions from Planet CubeSat images demonstrated great potential to monitor agricultural areas characterized by small individual-owned farmland and complex landscape. Thus, the data delivered from Planet CubeSat images contribute to overcome the trade-off between temporal and spatial resolution from satellite

data. Planet CubeSat images can subsidize, on forthcoming research, the regional and local monitoring of agricultural areas and contribute to the development of sustainable agricultural practices, providing valuable information for better management regarding strategical planning of governmental and corporative decision make over technical issues.

Disclosure statement

No potential conflict of interest was reported by the author(s).

Funding

This work was supported by the [Innovation Project of Chinese Academy of Agricultural Sciences] under Grant [960-3], [Fundamental Research Funds for the Chinese Academy of Agricultural Sciences] under Grant [Y2021GH18], [Talented Young Scientist Program – China Science and Technology Exchange Center] under Grant [Brazil – 19-004], the University College London Research Fund: AMAZING – Advancing Maize Information for Ghana [ST/V001388/1], and the [National Council for Scientific and Technological Development – CNPq].

ORCID

Luís Guilherme Teixeira Crusiol  <http://orcid.org/0000-0002-2387-964X>

Marcos Rafael Nanni  <http://orcid.org/0000-0003-4854-2661>

Data availability statement

Data associated with this paper is available with the correspondent author upon request.

References

- Aldeghi, A., S. Carn, R. Escobar-Wolf, and G. Groppelli. 2019. "Volcano Monitoring from Space Using High-cadence Planet CubeSat Images Applied to Fuego Volcano, Guatemala." *Remote Sensing* 11: 2151–2168. doi:10.3390/rs11182151.
- Aragon, B., R. Houborg, K. Tu, J. B. Fisher, and M. McCabe. 2018. "CubeSats Enable High Spatiotemporal Retrievals of Crop-water Use for Precision Agriculture." *Remote Sensing* 10: 1867–1888. doi:10.3390/rs10121867.
- Atkinson, P. M., C. Jeganathan, J. Dash, and C. Atzberger. 2012. "Inter-comparison of Four Models for Smoothing Satellite Sensor Time-series Data to Estimate Vegetation Phenology." *Remote Sensing of Environment* 123: 400–417. doi:10.1016/j.rse.2012.04.001.
- Bellón, B., A. Bégué, D. Lo Seen, C. A. De Almeida, and M. Simões. 2017. "A Remote Sensing Approach for Regional-scale Mapping of Agricultural Land-use Systems Based on NDVI Time Series." *Remote Sensing* 9: 600–616. doi:10.3390/rs9060600.
- Cooley, S. W., L. C. Smith, L. Stepan, and J. Mascaro. 2017. "Tracking Dynamic Northern Surface Water Changes with High-frequency Planet CubeSat Imagery." *Remote Sensing* 9: 1306–1326. doi:10.3390/rs9121306.
- Cui, T., L. Martz, L. Zhao, and X. Guo. 2020. "Investigating the Impact of the Temporal Resolution of MODIS Data on Measured Phenology in the Prairie Grasslands." *GIScience & Remote Sensing* 57: 395–410. doi:10.1080/15481603.2020.1723279.
- da Silva Junior, C. A., M. R. Nanni, P. E. Teodoro, and G. F. C. Silva. 2017. "Vegetation Indices for Discrimination of Soybean Areas: A New Approach." *Agronomy Journal* 109: 1331–1343. doi:10.2134/agnonj2017.01.0003.

- de Souza, C. H. W., E. Mercante, J. A. Johann, R. A. C. Lamparelli, and M. A. Uribe-Opazo. 2015. "Mapping and Discrimination of Soya Bean and Corn Crops Using Spectro-temporal Profiles of Vegetation Indices." *International Journal of Remote Sensing* 36: 1809–1824. doi:10.1080/01431161.2015.1026956.
- Dong, C., G. Zhao, Y. Qin, and H. Wan. 2019. "Area Extraction and Spatiotemporal Characteristics of Winter Wheat–summer Maize in Shandong Province Using NDVI Time Series." *PloS One* 14: e0226508. doi:10.1371/journal.pone.0226508.
- Draper, N. R., and H. Smith. 2014. *Applied Regression Analysis*, 736. 3rd ed. Hoboken: John Wiley Sons, New Jersey, United States of America.
- Furlanetto, R. H. 2018. "Sensores Multi E Hiperespectrais Na Identificação E Quantificação Da Deficiência De Potássio Na Cultura Do Milho (Zea Mays)". Dissertation, Universidade Estadual de Maringá.
- Gao, F., J. Masek, M. Schwaller, and F. Hall. 2006. "On the Blending of the Landsat and MODIS Surface Reflectance: Predicting Daily Landsat Surface Reflectance." *IEEE Transactions on Geoscience and Remote Sensing* 44: 2207–2218. doi:10.1109/TGRS.2006.872081.
- Hill, M. J., and G. E. Donald. 2003. "Estimating Spatio-temporal Patterns of Agricultural Productivity in Fragmented Landscapes Using AVHRR NDVI Time Series." *Remote Sensing of Environment* 84: 367–384. doi:10.1016/S0034-4257(02)00128-1.
- Holden, H., and E. LeDrew. 1998. "Spectral Discrimination of Healthy and Non-healthy Corals Based on Cluster Analysis, Principal Components Analysis, and Derivative Spectroscopy." *Remote Sensing of Environment* 65 (2): 217–224. doi:10.1016/S0034-4257(98)00029-7.
- Houborg, R., and M. F. McCabe. 2016. "High-resolution NDVI from Planet's Constellation of Earth Observing Nano-satellites: A New Data Source for Precision Agriculture." *Remote Sensing* 8: 768–786. doi:10.3390/rs8090768.
- Houborg, R., and M. F. McCabe. 2018. "A Cubesat Enabled Spatio-temporal Enhancement Method (Cestem) Utilizing Planet, Landsat and Modis Data." *Remote Sensing of Environment* 209: 211–226. doi:10.1016/j.rse.2018.02.067.
- Hu, Y., B. Li, Z. Zhang, and J. Wang. 2019. "Farm Size and Agricultural Technology Progress: Evidence from China." *Journal of Rural Studies*. doi:10.1016/j.jrurstud.2019.01.009.
- Huang, L., J. Luo, Z. Lin, F. Niu, and L. Liu. 2020. "Using Deep Learning to Map Retrogressive Thaw Slumps in the Beiluhe Region (Tibetan Plateau) from CubeSat Images." *Remote Sensing of Environment* 237: 111534. doi:10.1016/j.rse.2019.111534.
- Jolliffe, I. T., and J. Cadima. 2016. "Principal Component Analysis: A Review and Recent Developments." *Philosophical Transactions of the Royal Society A* 374: 20150202. doi:10.1098/rsta.2015.0202.
- Kääb, A., B. Altena, and J. Mascaro. 2017. "Coseismic Displacements of the 14 November 2016 Mw 7.8 Kaikoura, New Zealand, Earthquake Using the Planet Optical Cubesat Constellation." *Natural Hazard Earth System Science* 17: 627–639. doi:10.5194/nhess-17-627-2017.
- Karimi, Y., S. O. Prasher, H. Mcnairn, R. B. Bonnell, P. Dutilleul, and P. K. Goel. 2005. "Classification Accuracy of Discriminant Analysis, Artificial Neural Networks, and Decision Trees for Weed and Nitrogen Stress Detection in Corn." *Transactions of the ASAE* 48: 261–268. doi:10.13031/2013.18490.
- Kimm, H., K. Guan, C. Jiang, B. Peng, L. F. Gentry, S. C. Wilkin, S. Wang, et al. 2020. "Deriving High-spatiotemporal-resolution Leaf Area Index for Agroecosystems in the US Corn Belt Using Planet Labs CubeSat and STAIR Fusion Data." *Remote Sensing of Environment* 239: 111615. doi:10.1016/j.rse.2019.111615.
- Li, J., and D. P. Roy. 2017. "A Global Analysis of Sentinel-2A, Sentinel-2B and Landsat-8 Data Revisit Intervals and Implications for Terrestrial Monitoring." *Remote Sensing* 9: 902. doi:10.3390/rs9090902.
- Li, J., S. R. Schill, D. E. Knapp, and G. P. Asner. 2019. "Object-Based Mapping of Coral Reef Habitats Using Planet Dove Satellites." *Remote Sensing* 11: 1445–1460. doi:10.3390/rs11121445.
- Li, X., F. Ling, G. M. Foody, Y. Ge, Y. Zhang, and Y. Du. 2017. "Generating a Series of Fine Spatial and Temporal Resolution Land Cover Maps by Fusing Coarse Spatial Resolution Remotely Sensed

- Images and Fine Spatial Resolution Land Cover Maps." *Remote Sensing of Environment*: 196: 293–311. doi:10.1016/j.rse.2017.05.011.
- Li, X., Y. He, and H. Fang. 2007. "Non-destructive Discrimination of Chinese Bayberry Varieties Using Vis/NIR Spectroscopy." *Journal of Food Engineering* 81 (2): 357–363. doi:10.1016/j.jfoodeng.2006.10.033.
- Liang, S. Z., Ma, W. D., Sui, X. Y., Yao, H. M., Li, H. Z., Liu, T., H. X., Wang, M. 2017. „Extracting the spatiotemporal pattern of cropping systems from NDVI time series using a combination of the spline and HANTS Algorithms: A case study for Shandong Province,„ *Canadian Journal of Remote Sensing* 43: 1–15. doi:10.1080/07038992.2017.1252906
- Liu, L., X. Zhang, Y. Yu, F. Gao, and Z. Yang. 2018. "Real-time Monitoring of Crop Phenology in the Midwestern United States Using VIIRS Observations." *Remote Sensing* 10: 1540–1557. doi:10.3390/rs10101540.
- Liu, M., W. Yang, X. Zhu, J. Chen, X. Chen, L. Yang, and E. H. Helmer. 2019. "An Improved Flexible Spatiotemporal DATA Fusion (IFSDAF) Method for Producing High Spatiotemporal Resolution Normalized Difference Vegetation Index Time Series." *Remote Sensing of Environment* 227: 74–89. doi:10.1016/j.rse.2019.03.012.
- Liu, Y., R. Xie, P. Hou, S. Li, H. Zhang, B. Ming, H. Long, and S. Liang. 2013. "Phenological Responses of Maize to Changes in Environment When Grown at Different Latitudes in China." *Field Crops Research* 144: 192–199. doi:10.1016/j.fcr.2013.01.003.
- Löw, F., and G. Duveiller. 2014. "Defining the Spatial Resolution Requirements for Crop Identification Using Optical Remote Sensing." *Remote Sensing* 6: 9034–9063. doi:10.3390/rs6099034.
- Maciel, D. A., E. M. L. D. M. Novo, C. C. F. Barbosa, V. S. Martins, R. Flores Júnior, A. H. Oliveira, L. A. S. De Carvalho, and F. D. L. Lobo. 2020. "Evaluating the Potential of CubeSats for Remote Sensing Reflectance Retrieval over Inland Waters." *International Journal of Remote Sensing* 41: 2807–2817. doi:10.1080/2150704X.2019.1697003.
- Masialeli, I., S. Egbert, and B. D. Wardlow. 2010. "A Comparative Analysis of Phenological Curves for Major Crops in Kansas." *GIScience & Remote Sensing* 47: 241–259. doi:10.2747/1548-1603.47.2.241.
- Mazzanti, P., P. Caporossi, and R. Muzi. 2020. "Sliding Time Master Digital Image Correlation Analyses of CubeSat Images for Landslide Monitoring: The Rattlesnake Hills Landslide (USA)." *Remote Sensing* 12: 592–606. doi:10.3390/rs12040592.
- Myers, E., J. Kerekes, C. Daughtry, and A. Russ. 2019. "Assessing the Impact of Satellite Revisit Rate on Estimation of Corn Phenological Transition Timing through Shape Model Fitting." *Remote Sensing* 11: 2558–2578. doi:10.3390/rs11212558.
- Padhee, S. K., and S. Dutta. 2019. "Spatio-temporal Reconstruction of MODIS NDVI by Regional Land Surface Phenology and Harmonic Analysis of Time-series." *GIScience & Remote Sensing* 56: 1261–1288. doi:10.1080/15481603.2019.1646977.
- Pan, Z., J. Huang, Q. Zhou, L. Wang, Y. Cheng, H. Zhang, G. A. Blackburn, L. Yan, and J. Liu. 2015. "Mapping Crop Phenology Using NDVI Time-series Derived from HJ-1 A/B Data." *International Journal of Applied Earth Observation and Geoinformation* 34: 188–197. doi:10.1016/j.jag.2014.08.011.
- Pax-Lenney, M., and C. E. Woodcock. 1997. "The Effect of Spatial Resolution on the Ability to Monitor the Status of Agricultural Lands." *Remote Sensing of Environment* 61: 210–220. doi:10.1016/s0034-4257(97)00003-5.
- Peña, M. A., and A. Brenning. 2015. "Assessing Fruit-tree Crop Classification from Landsat-8 Time Series for the Maipo Valley, Chile." *Remote Sensing of Environment* 171: 234–244. doi:10.1016/j.rse.2015.10.029.
- Poursanidis, D., D. Traganos, N. Chrysoulakis, and P. Reinartz. 2019. "Cubesats Allow High Spatiotemporal Estimates of Satellite-derived Bathymetry." *Remote Sensing* 11: 1299–1310. doi:10.3390/rs11111299.
- Qiu, B., M. Feng, and Z. Tang. 2016. "A Simple Smoother Based on Continuous Wavelet Transform: Comparative Evaluation Based on the Fidelity, Smoothness and Efficiency in Phenological Estimation." *International Journal of Applied Earth Observation and Geoinformation* 47: 91–101. doi:10.1016/j.jag.2015.11.009.

- Rouse, J. W., R. H. Haas, J. A. Schell, and D. W. Deering. 1974. "Monitoring Vegetation Systems in the Great Plains with ERTS." *NASA Special Publication* 351: 309.
- Sakamoto, T. 2020. "Incorporating Environmental Variables into a MODIS-based Crop Yield Estimation Method for United States Corn and Soybeans through the Use of a Random Forest Regression Algorithm." *ISPRS Journal of Photogrammetry and Remote Sensing* 160: 208–228. doi:10.1016/j.isprsjprs.2019.12.012.
- Shao, X., S. Ma, C. Xu, P. Zhang, B. Wen, Y. Tian, Q. Zhou, and Y. Cui. 2019. "Planet Image-based Inventorying and Machine Learning-based Susceptibility Mapping for the Landslides Triggered by the 2018 Mw6.6 Tomakomai, Japan Earthquake." *Remote Sensing* 11: 978–1000. doi:10.3390/rs11080978.
- Shimizu, K., T. Ota, N. Mizoue, and H. Saito. 2020. "Comparison of Multi-temporal PlanetScope Data with Landsat 8 and Sentinel-2 Data for Estimating Airborne LiDAR Derived Canopy Height in Temperate Forests." *Remote Sensing* 12: 1876. doi:10.3390/rs12111876.
- Song, X. P., P. V. Potapov, A. Krylov, L. King, C. M. Di Bella, A. Hudson, A. Khan, B. Adusei, S. V. Stehman, and M. C. Hansen. 2017. "National-scale Soybean Mapping and Area Estimation in the United States Using Medium Resolution Satellite Imagery and Field Survey." *Remote Sensing of Environment* 190: 383–395. doi:10.1016/j.rse.2017.01.008.
- Straw, C. M., and G. M. Henry. 2018. "Spatiotemporal Variation of Site-specific Management Units on Natural Turfgrass Sports Fields during Dry Down." *Precision Agriculture* 19: 395–420. doi:10.1007/s11119-017-9526-5.
- Sun, L., F. Gao, D. Xie, M. Anderson, R. Chen, Y. Yang, Y. Yang, and Z. Chen. 2021. "Reconstructing Daily 30 M NDVI over Complex Agricultural Landscapes Using a Crop Reference Curve Approach." *Remote Sensing of Environment* 253: 112156. doi:10.1016/j.rse.2020.112156.
- Sun, L., F. Gao, M. C. Anderson, W. P. Kustas, M. M. Alsina, L. Sanchez, B. Sams, et al.. 2017. "Daily Mapping of 30 M LAI and NDVI for Grape Yield Prediction in California Vineyards." *Remote Sensing* 9: 317–334. doi:10.3390/rs9040317.
- Thenkabail, P. S., E. A. Enclona, M. S. Ashton, and B. Van Der Meer. 2004. "Accuracy Assessments of Hyperspectral Waveband Performance for Vegetation Analysis Applications." *Remote Sensing of Environment* 91: 354–376. doi:10.1016/j.rse.2004.03.013.
- Tsalyuk, M., M. Kelly, and W. M. Getz. 2017. "Improving the Prediction of African Savanna Vegetation Variables Using Time Series of MODIS Products." *ISPRS Journal of Photogrammetry and Remote Sensing* 131: 77–91. doi:10.1016/j.isprsjprs.2017.07.012.
- USDA (United States Department of Agriculture). 2020. "World Agricultural Production. Circular Series WAP 5-20, May 2020". <https://apps.fas.usda.gov/psdonline/circulars/production.pdf>.
- Vrieling, A., A. K. Skidmore, T. Wang, M. Meroni, B. J. Ens, K. Oosterbeek, B. O'Connor, et al.. 2017. "Spatially Detailed Retrievals of Spring Phenology from Single-season High-resolution Image Time Series." *International Journal of Applied Earth Observation and Geoinformation* 59: 19–30. doi:10.1016/j.jag.2017.02.021.
- Wang, H. W. 1999. *Partial Least Squares Regression Method and Applications*, 274. Beijing, China: National Defense Industry Press.
- Wardlow, B. D., S. L. Egbert, and J. H. Kastens. 2007. "Analysis of Time-series MODIS 250 M Vegetation Index Data for Crop Classification in the US Central Great Plains." *Remote Sensing of Environment* 108: 290–310. doi:10.1016/j.rse.2006.11.021.
- Werner, J. P. S., S. D. M. Oliveira, and J. C. D. M. Esquerdo. 2020. "Mapping Cotton Fields Using Data Mining and MODIS Time-series." *International Journal of Remote Sensing* 41: 2457–2476. doi:10.1080/01431161.2019.1693072.
- Wicaksono, P., and W. Lazuardi. 2018. "Assessment of PlanetScope Images for Benthic Habitat and Seagrass Species Mapping in a Complex Optically Shallow Water Environment." *International Journal of Remote Sensing* 39: 5739–5765. doi:10.1080/01431161.2018.1506951.
- Wu, Y., X. Xi, X. Tang, D. Luo, B. Gu, S. K. Lam, P. M. Vitousek, and D. Chen. 2018. "Policy Distortions, Farm Size, and the Overuse of Agricultural Chemicals in China." *Proceedings of the National Academy of Sciences* 115: 7010–7015. doi:10.1073/pnas.1806645115.

- Zeng, L., B. D. Wardlow, D. Xiang, S. Hu, and D. Li. 2020. "A Review of Vegetation Phenological Metrics Extraction Using Time-series, Multispectral Satellite Data." *Remote Sensing of Environment* 237: 111511. doi:[10.1016/j.rse.2019.111511](https://doi.org/10.1016/j.rse.2019.111511).
- Zhang, X., J. Wang, G. M. Henebry, and F. Gao. 2020. "Development and Evaluation of a New Algorithm for Detecting 30 M Land Surface Phenology from VIIRS and HLS Time Series." *ISPRS Journal of Photogrammetry and Remote Sensing* 161: 37–51. doi:[10.1016/j.isprsjprs.2020.01.012](https://doi.org/10.1016/j.isprsjprs.2020.01.012).
- Zhou, F., A. Zhang, and L. Townley-Smith. 2013. "A Data Mining Approach for Evaluation of Optimal Time-series of MODIS Data for Land Cover Mapping at A Regional Level." *ISPRS Journal of Photogrammetry and Remote Sensing* 84: 114–129. doi:[10.1016/j.isprsjprs.2013.07.008](https://doi.org/10.1016/j.isprsjprs.2013.07.008).
- Zhou, J., L. Jia, and M. Menenti. 2015. "Reconstruction of Global MODIS NDVI Time Series: Performance of Harmonic ANalysis of Time Series (HANTS)." *Remote Sensing of Environment* 163: 217–228. doi:[10.1016/j.rse.2015.03.018](https://doi.org/10.1016/j.rse.2015.03.018).
- Zhou, J., L. Jia, M. Menenti, and B. Gorte. 2016. "On the Performance of Remote Sensing Time Series Reconstruction methods—A Spatial Comparison." *Remote Sensing of Environment* 187: 367–384. doi:[10.1016/j.rse.2016.10.025](https://doi.org/10.1016/j.rse.2016.10.025).
- Zhu, X., E. H. Helmer, F. Gao, D. Liu, J. Chen, and M. Lefsky. 2016. "A Flexible Spatiotemporal Method for Fusing Satellite Images with Different Resolutions." *Remote Sensing of Environment* 172: 165–177. doi:[10.1016/j.rse.2015.11.016](https://doi.org/10.1016/j.rse.2015.11.016).
- Zhu, X., J. Chen, F. Gao, X. Chen, and J. G. Masek. 2010. "An Enhanced Spatial and Temporal Adaptive Reflectance Fusion Model for Complex Heterogeneous Regions." *Remote Sensing of Environment* 114: 2610–2623. doi:[10.1016/j.rse.2010.05.032](https://doi.org/10.1016/j.rse.2010.05.032).